Proceeding Paper

Recycling-Oriented Design of the Al-Zn-Mg-Ca Alloys [†]

Pavel Shurkin [1],*, Nikolay Belov [1], Torgom Akopyan [1] and Zhanna Karpova [1,2]

[1] Department of Metal Forming, National University of Science and Technology MISiS, 119049 Moscow, Russia; nikolay-belov@yandex.ru (N.B.); nemiroffandtor@yandex.ru (T.A.); zkarpova2012@yandex.ru (Z.K.)

[2] Keldysh Research Center, 119049 Moscow, Russia

* Correspondence: pa.shurkin@gmail.com; Tel.: +7-926-585-1990

[†] Presented at the 1st International Electronic Conference on Metallurgy and Metals, 22 February–7 March 2021; Available online: https://iec2m.sciforum.net/.

Abstract: Approaches to the design of recycling-tolerant Al-Zn-Mg alloys were formulated to be achieved via combined Ca, Fe, and Si, and appropriate solidification conditions and heat treatment. A CalPhaD calculation and experimental study were employed for analysis of the Al-8%Zn-3%Mg alloy doped with 1–2%Ca, 0.5%Fe, and 0.5%Si. The Al-8%Zn-3%Mg-1%Ca-0.5%Fe-0.5%Si (AlZnMg1CaFeSi) alloy was preliminarily found to be promising since it showed a high equilibrium solidus, and an as-cast structure including curved phases (Al), Al_3Fe, Al_2CaSi_2, $Al_{10}CaFe_2$, and (Al, Zn)$_4$Ca; favouring a further spheroidization response during a two-step annealing at 450 °C, 3 h + 520 °C, 3 h. Furthermore, the alloy showed an excellent age-hardening response (195 HV, T6), which did not yield the values of the base alloy and outperformed the values of the other experimental counterparts. Regarding feasibility, 80% reduction hot rolling was successfully conducted, as well as a brief comparison with commercial 6063 impurity-tolerant alloys. As it showed qualitatively similar structural patterns and Fe and Si alloying opportunities, the AlZnMg1CaFeSi alloy may serve as a sustainable basis for the further development of high-strength aluminum alloys tailored for manufacture from scrap materials.

Keywords: Al-Zn-Mg-Ca alloys; iron; silicon; recycling; phase composition; microstructure

1. Introduction

The role of recycling in metallurgical engineering has always been essential and prevalent, having a critical impact not only on the global economy and energy consumption but also on the ecological environment and human life. This is due to opportunities for reducing primary metal manufacturing, which is commonly accompanied by hazardous waste and greenhouse gases emissions [1]. When considering aluminum and its alloys, their recycling is recognized to be the mature engine of recycling economics, which is constantly developing under new technological approaches toward shredding, sorting, and castshop manufacturing [2,3]. However, though recycling has made advances, the consumption of primary aluminum has kept at a high level (70% primary, 30% recycled), which is mostly sustained by demand for premium wrought alloys, intolerant to impurities [1,4,5]. Specifically, the strongest 7xxx (Al-Zn-Mg) alloys show a marked loss of ductility when Fe and Si impurities are present, due to the formation of harmful intermetallics (β type phases), Al_3Fe, Al_5FeSi, and Al_7Cu_2Fe, which appear as faceted platelets of up to several millimetres [6–8]. We find it drastic but expedient to develop new aluminum alloys which are tolerant of the aforementioned impurities.

Current research on the development of secondary aluminum alloys often bypasses the 7xxx family alloys, and thus, most of the new compositions are not able to replicate its high strength. Some part of material scientists make a point of recycling chips from the same family via powder metallurgy, and also may include work on the addition of rein-

forcement particles [9] and severe plastic deformation [10], but there is no sense of impurities and sustainability for industrial scaling. Meanwhile, the Fe and Si determine the performance of the alloy, not only in mechanical properties but also in corrosion resistance and physical properties, like density [8,11–13].

The available machine learning equipment and thermodynamic databases are already used for designing lightweight steels, sustainable materials for additive manufacturing, and high-entropy materials. The approach used for years is phase diagram calculation (CalPhaD), providing projections on how the alloy would solidify or melt. In this sense, it seems to be possible to design a universal high-strength aluminum alloy using low-concentrations of multiple-element aluminum corners constructed using both the available data on multicomponent diffusion capacity and intermetallics range and an experimental approach on a micro-and near-atomic scale. In favor of this approach, many works have been performed on calculating an Al-Zn-Mg-Ni-Fe system, and promoting new alloys with a justified Ni/Fe ratio of 1:1, allowing the formation of 5 vol.% of fine Al_9FeNi phase [14–16]. However, Nickel is not allowed in recycling-oriented plants as it is a very expensive material. Calcium seems to be far more preferential since it is the third most abundant metal in the earth's crust. Recently, several works on Al-Ca-Fe-Si alloys showed that calcium may bind the impurities into finely shaped ternary phases, $Al_{10}CaFe_2$ and Al_2CaSi_2 [17,18]. In our recent research on Al-Zn-Mg-Ca-Fe [19] and Al-Zn-Mg-Ca-Si [20] alloys we showed that the foregoing phases may appear as a very fine constituent. However, joint Ca, Fe, and Si alloying has not yet been considered.

Having made the foregoing statements, this study aimed to describe the approaches to designing recycling-oriented Al-Zn-Mg-Ca alloys and to present the preliminary results on the microstructure, hardening, and feasibility of Al-Zn-Mg-Ca-Fe-Si alloys. The results may bring huge progress into a currently static field, for the recyclability of high-strength aluminum alloys.

2. Materials and Methods

Six model compositions based on the Al-8%Zn-3%Mg matrix were chosen for investigation. For the sake of demonstration of the joint alloying effect, we studied the base matrix alloy, Ca-free alloy doped with Fe and Si, and alloys doped with different Ca. Their chemical compositions, according to spectral analysis, are given in Table 1.

Table 1. Chemical compositions of the model alloys as determined by spectral analysis.

Alloy	Nominal and Actual Concentrations (in Brackets), wt.%					
	Zn	Mg	Ca	Fe	Si	Al
AlZnMg	8(8.1)	3 (2.8)	0	0	0	Balance
AlZnMgFeSi	8 (7.9)	3 (2.9)	0	0.5(0.51)	0.5(0.49)	Balance
AlZnMg1Ca	8 (7.7)	3 (2.6)	1(0.9)	0	0	Balance
AlZnMg2Ca	8 (7.8)	3 (3.1)	2(1.8)	0	0	Balance
AlZnMg1CaFeSi	8 (8.0)	3 (2.8)	1(0.9)	0.5(0.55)	0.5(0.51)	Balance
AlZnMg2CaFeSi	8 (7.7)	3 (2.9)	2(1.9)	0.5(0.52)	0.5(0.50)	Balance

The CALPHAD (Calculation phase diagram) approach implemented in Thermo-Calc software (Version 3.1, TCAl4 Al-based alloy database, Thermo-Calc Software AB, 81 Stockholm, Sweden) [21] was employed for analysis of phase composition and solidification behaviour. It was also used for substantiating the alloy content and heat treatment route, shown further in the results section.

The experimental alloys were prepared by the melting route in an electric resistance furnace, Nabertherm K 1/13 (Nabertherm GmbH, 71 Lilienthal, Germany), using a 500 g capacity graphite crucible. The melting was carried out in an air atmosphere, without the addition of protective gas. High-purity (99.99%) and commercially pure (99.9%) alumi-

num were employed as starting materials for Fe- and Si-free alloys and other alloys, respectively. Following the melting of the aluminum bulk, master alloys Al15%Ca, Al10%Fe, and Al10%Si were added with continuous manual stirring down to their dissolution. Then, pure Zn (99.99%) and Mg (99.99%) were added, followed by homogenization for 15 min at 730–750 °C, skimming, and pouring into a steel mould 15 × 60 × 180 mm. The cooling rate was approximately 40 °C/s, as it was estimated by a single-thermocouple plugged into an AKTAKOM-2006 recording unit. The latter technique was also used for thermal analysis of the ~50 g samples slowly cooled in the furnace atmosphere.

Heat treatment of the samples included two-step annealing (450 °C, 3 h + 520 °C, 3 h) and quenching in water (hereinafter referred to as T4), which will be approved in the results section. Ageing was performed as isochronal low-temperature exposure at 175°C for 3 h that corresponded to the T6 condition [19,20]. The microstructure was examined in as-cast and T4 conditions by scanning electron microscopy (SEM, TESCAN VEGA3), with an electron microprobe analysis system (EMPA, Oxford Instruments) and Aztec software. The samples were prepared by polishing with diamond suspension and electrochemical etching (6 C_2H_5OH, 1 $HClO_4$, 1 glycerin). To control the properties evolved, Vickers' hardness test at a load of 10 g (0.1 N) and 15 s dwell was used.

3. Results

3.1. Principles of the Alloy Design

Before starting on the experimental investigations, the approaches to designing novel alloys will be briefly clarified. In general, the main principles were taken from [8,14,16], which described a highly consistent action for increasing impurities by developing multi-phase eutectic structures. In these works, they proposed searching for existing eutectic mixtures, including differentiated Fe-bearing phase Al_8Fe_2Si, Al_9FeNi, and $Al_{16}Fe_4Be_3Si_2$, along with (Si) or Mg_2Si available in particular alloys based on Al-Fe-Mg-Si, Al-Fe-Ni-Si, and Al-Fe-Be-Mg-Si. Moreover, there are some recent works on Al-Ca-Fe-Si alloys containing an (Al)+Al_4Ca+$Al_{10}CaFe_2$+Al_2CaSi_2 eutectic mixture. Regarding the essential formation of multiphase eutectic, it is stipulated by substantial differentiation of the structure due to the increase in the net volume fraction of the eutectic phases, and providing a similar effect as due to an increase in cooling rate. Indeed, the latter must also be controlled as a part of the tuning solidification behaviour that must provide an appropriate structure, compatible with further treatment. The next step after solidification is the homogenization treatment for stress relief, dissolving of non-equilibrium phases, and favourable shaping of the insoluble phases. The latter, for example, is widely used in 6xxx alloys for the β-Fe phase to α-Fe phase transformation, and the efficiency is dependent on the initial phase morphology. Schematic structure evolution in two-phase and three-phase eutectic alloys is presented in Figure 1.
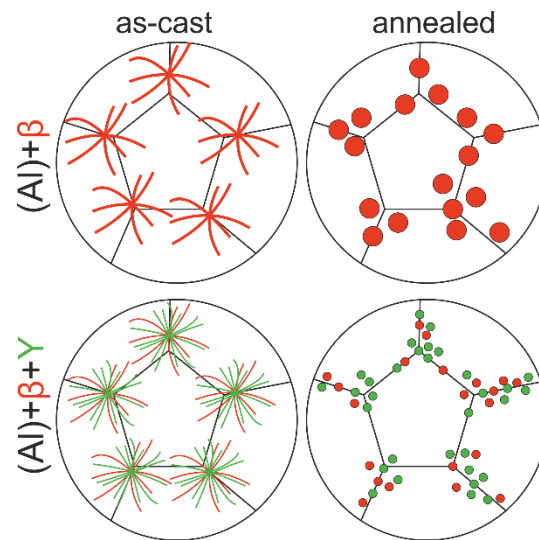
Figure 1. Schematic view of the two-phase and three-phase eutectics in as-cast and annealed conditions.

While the smooth surface of a needle- or plate-like Al_3Fe and Al_5FeSi phases is not stable against heating (even near solidus), the curved skeleton-like phases, particularly $Al_{10}CaFe_2$ and Al_2CaSi_2, may be fragmented or even spheroidized after exposure to 450–500 °C, due to far higher surface energy. Ultimately, the methods we followed for neutralization of the harmful recycling-originated Fe and Si impurities were as the following: (1) appropriate alloying and solidification conditions for achieving a multiphase eutectic with curved intermetallics inside, and (2) substantial heating near solidus for achieving globular and uniformly distributed intermetallics, favouring ductility at metal formation.

3.2. Substantiation of the Alloying Content and Heat Treatment Route

When considering Al-Zn-Mg alloys, several works [14–16] used the foregoing principles for developing Fe-rich compositions via Ni alloying and providing Al_9FeNi phase formation. While the results were successful, the alloying approach may not be described as sustainable for practical applications, as nickel is an expensive element. Calcium is abundant in the Earth's crust and also very versatile in aluminide formation, specifically $Al_{10}CaFe_2$ and Al_2CaSi_2, favouring flexibility in recycling-tolerant Al-Zn-Mg-Ca alloy design. Based on the available information [17–20], seven phases containing Ca, Fe, and Si ((Al, $Zn)_4Ca$, $Al_{10}CaFe_2$, Al_2CaSi_2, Al_3Fe, Al_8Fe_2Si, Al_5FeSi, and Mg_2Si) may be in equilibrium with (Al) in the alloys of the considered system. The most probable distribution of the elements among these phases is given in Table 2. It can be seen that Ca, Fe, and Si additives do not form precipitates. Therefore, the hardening effect of the multi-component alloy depends on the concentrations of Zn and Mg in (Al) before ageing (after quenching).

Table 2. Distribution of elements among phases in the Al-Zn-Mg-Ca-Fe-Si alloys.

Phases	Element					
	Al	**Zn**	**Mg**	**Ca**	**Fe**	**Si**
Phases forming during solidification						
$(Al,Zn)_4Ca$	+	+	-	+	-	-
$Al_{10}CaFe_2$	+	-	-	+	+	-
Al_2CaSi_2	+	-	-	+	-	+
Al_3Fe	+	-	-	-	+	-
α-Fe (Al_8Fe_2Si)	+	-	-	-	+	+
β-Fe (Al_5FeSi)	+	-	-	-	+	+
Mg_2Si	-	-	+	-	-	+

T (Al$_2$Mg$_3$Zn$_3$)	+	+	+	-	-	-
M (MgZn$_2$)	-	+	+	-	-	-
Precipitates						
T (Al$_2$Mg$_3$Zn$_3$)	+	+	+	-	-	-
M (MgZn$_2$)	-	+	+	-	-	-

Unfortunately, the currently available CALPHAD databases do not count the existence of the Al$_{10}$CaFe$_2$ phase and the solubility of Zn in the (Al, Zn)$_4$Ca phase. However, as our previous research on Al-Zn-Mg-Ca-Fe alloys [19] showed, the foregoing phases may appear as a result of non-equilibrium solidification induced by the casting cooling rate, while slow-cooled samples included Al$_3$Fe intermetallics. This case is quite similar to Al-Fe-Mg-Si alloys, which may exhibit the Al$_8$Fe$_2$Si phase instead of the Al$_5$FeSi phase upon an accelerated cooling rate [8]. Having said that, the calculation data must be strongly supported by experimental evaluation. Preliminary, we provide several principles supported by our previous research on Al-Zn-Mg and Ca-rich aluminum alloys and CALPHAD calculation:

(1) Zn and Mg must provide a more than sufficient hardening after solid solution treatment and ageing. With regards to further practical applications, their amount (8 wt.% and 3 wt.%) was chosen from concentrations in the established ultra-high-strength 7085 alloy and our previous studies. For example, the latter showed that excessive Zn (>10 wt.%) may bring a lowering of equilibrium solidus and further grain-boundary melting after homogenizing annealing at 500 °C. Additionally, several works [22–24] have revealed that an increase in Zn content over 9 wt.% causes a decrease in ductility, rather than an increase in strength. When considering Mg, the content chosen was the maximum for commercial alloys [25]. An increase in Mg is practically used for increasing hot tearing resistance, while the toughness, essential for wrought alloys, may be tuned by lowering the Mg:Zn ratio. In addition, as is shown in Figure 2a both Zn and Mg remarkably narrow the area of (Al) solidification. However, Zn acts in a slightly stronger manner and may bring some risks regarding an unacceptable primary solidification of intermetallics.

(2) Ca provides the formation of the eutectic-origin phases, which may also include Fe and Si (Al$_{10}$CaFe$_2$, Al$_2$CaSi$_2$). An increase in the Ca content may bring far more benefits in improving density, corrosion resistance, and casting properties. However, to the best of our knowledge, the Ca content must be controlled down to 2 wt.% due to limitations in industrial emission spectrometry for chemical analysis. Besides, the higher the Ca, the lower the Zn in (Al), due to the incrementing (Al, Zn)$_4$Ca phase, bringing a loss of strength. In addition to the primary solidification, an increase in Ca from 1 wt.% to 2 wt% shifts the equilibrium line Al$_3$Fe/(Al) by 0.12 wt.%. Hence, further Ca alloying may bring Fe-bearing primary phase at a given Fe and Si content.

(3) Fe and Si contents each of 0.5 wt.% were chosen for the sake of sustainability, providing opportunities to use commercially pure primary aluminum (Fe + Si < 0.5 wt.%), packing, or electrical scrap of grades like 1100 and 8176 (Fe + Si < 1 wt.%). Indeed, these elements aggravate the performance of the alloy mainly due to the possible formation of adverse Al$_3$Fe and Mg$_2$Si phases. According to preliminary calculations, even if the formation of the Al$_8$Fe$_2$Si could be achieved by an increase in Si content, it also would lead to excessive Mg$_2$Si phase and lowering of the effective Mg in Al. In this respect, based on our previous studies we advocated speculating on the beneficial Ca effect for favouring the microstructure due to the formation of ternary phases.

According to the polythermal section displayed in Figure 2b, the multicomponent Al-Zn-Mg-Ca-Fe-Si alloys undergo complicated phase transformations during equilibrium solidification included mainly eutectic-based precipitations from the liquid and further solid-state transformations including the formation of T and M phases and Mg$_2$Si phases.
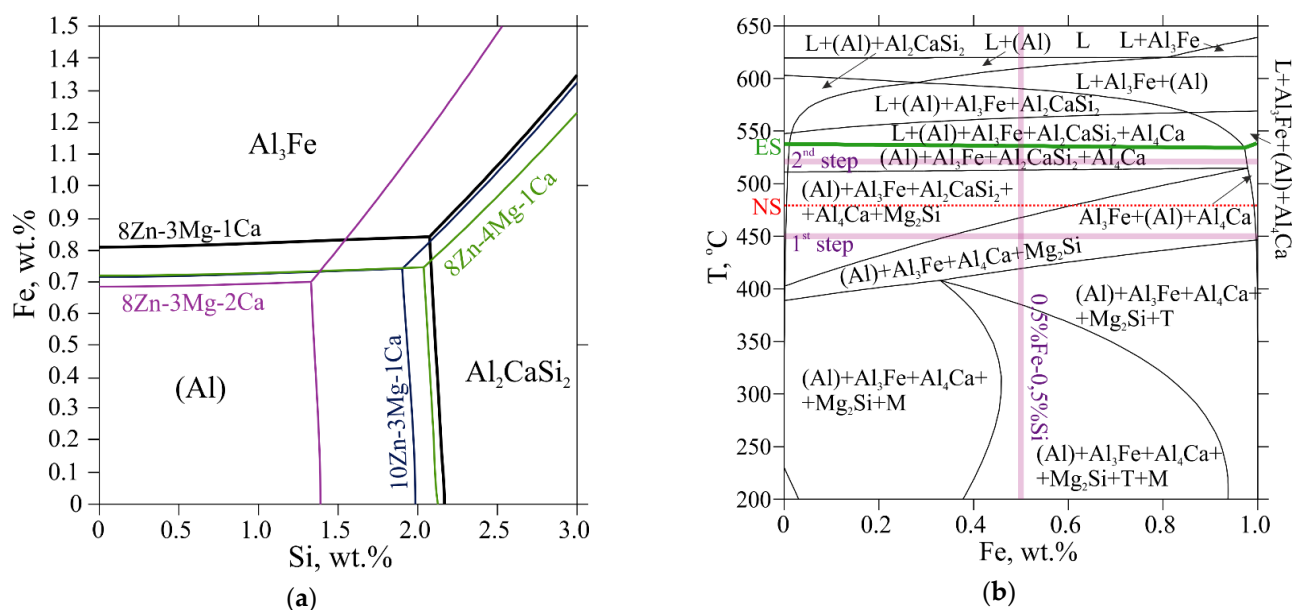
Figure 2. Calculation phase diagram (CALPHAD) calculation results: (**a**) liquidus projections of the Al-Zn-Mg-Ca-Fe-Si system at 8–10% Zn, 3–4%Mg, 1–2% Ca; (**b**) polythermal section of the Al-Zn-Mg-Ca-Fe-Si system at 8% Zn, 3% Mg, 1% Ca and 1% (Fe + Si).

By varying Fe:Si ratio it is possible to extend the cooling ranges for the Al_3Fe (or preferably $Al_{10}CaFe_2$) phase or Al_2CaSi_2 phase formation. Moreover, this ratio influences the Mg_2Si solid-state transformation in the five-phase field $(Al)+Al_3Fe+Al_2CaSi_2+Al_4Ca+Mg_2Si$. However, the latter is not expected as it would require the decay of the Al_2CaSi_2 phase, impossible due to the low diffusion of Ca. Moreover, the formation of the Mg_2Si in Al-Mg-Ca-Si alloys proceeds via peritectic reaction, $L+Al_2CaSi_2 \rightarrow (Al)+Al_4Ca+Mg_2Si$ [17], which might be suppressed in actual solidification conditions. As we chose equal concentrations of 0.5% Fe and 0.5% Si, cooling range equality (~40 °C) between Al_3Fe ($Al_{10}CaFe_2$) and Al_2CaSi_2 precipitations was expected. Indeed, it was preferable to obtain cast samples completely solidified at ~540 °C (equilibrium solidus, the green line in Figure 2b), according to the equilibrium path in the $(Al)+Al_3Fe(Al_{10}CaFe_2)+Al_2CaSi_2+Al_4Ca((Al, Zn)_4Ca)$ phase field. In that sense, the alloy would have excellent casting properties and may be compatible with high-temperature homogenization for shape tuning of the intermetallics. However, under non-equilibrium (actual) solidification conditions, the alloy remains liquid until the precipitation of T and M phases at ~480 °C (non-equilibrium solidus, the red dotted line in Figure 2b). This was calculated by Scheil–Gulliver simulation, which confirmed that the solidification range increases from ~80 °C to ~140 °C due to the formation of the non-equilibrium eutectic. This path is a key technological factor in 7xxx alloys, determining their service temperatures and limited casting properties. It should be mentioned that the latter may be improved by the addition of eutectic-forming elements like Ca, due to crack-healing factors and the reduction in effective solidification range, as is shown in [26].

Summing up the calculation results, in terms of alloys design, we chose the alloying content that provided a sufficiently high solidus temperature, which is achieved only in equilibrium conditions. This factor forced us to use a two-step annealing mode. According to the results of the thermal analysis, the actual temperatures were consistent with the calculated ones (Table 3). This follows the rules, as the increase in alloying content leads to a decrease in liquidus and formation of the curvatures related to phase precipitations. It can be noticed, that AlZnMg2CaFeSi does not show the formation of the non-equilibrium eutectic, which was probably due to excessive Ca content and extended dissolving Zn in the (Al, Zn)$_4$Ca phase; unfavourable to further solid solution and age-hardening. Nevertheless, the results allowed us to profoundly substantiate the chosen heat treatment

route including two-step annealing 450 °C, 3 h + 520 °C, 3 h, which also proved to be efficient in our previous studies. The first step aims to dissolve the non-equilibrium Zn- and Mg-bearing non-equilibrium eutectic (mainly, T and M phase mixture) and falls into the $(Al)+Al_3Fe(Al_{10}CaFe_2)+Mg_2Si+Al_4Ca((Al, Zn)_4Ca)$ field in the polythermal section. The second step ensures the absence of the Mg_2Si since it falls into the $(Al)+Al_3Fe(Al_{10}CaFe_2)+Al_2CaSi_2+Al_4Ca((Al, Zn)_4Ca)$ phase field, and might be effective in shape tuning of the insoluble intermetallics with Ca, Fe, and Si up to their spheroidization.

Table 3. Transformation temperatures in the model alloys, as determined by calculation and direct thermal analysis.

Alloy	Phase Transformation Temperatures (Calculation/Experimental), °C [1]							
	L [1]	Al₃Fe [2]	Mg₂Si	Al₄Ca [3]	Al₂CaSi₂	T	NS [2]	ES [2]
AlZnMg	632/628					483/474	482	559
AlZnMgFeSi	627/623	615/613	564/561			480/471	474	560
AlZnMg1Ca	626/623			566/589		482/470	478	545
AlZnMg2Ca	619/617			578/594		482/468	477	540
AlZnMg1CaFeSi	620/616	610/-	526/-	559/-	589/585	482/468	477	538
AlZnMg2CaFeSi	613/610	605/-	526/-	574/-	591/598	481/-	478	535

[1] L—liquidus; NS—non-equilibrium solidus; ES—equilibrium solidus; [2] $Al_{10}CaFe_2$ as expected in actual solidification conditions; [3] $(Al, Zn)_4Ca$ as expected in actual solidification conditions.

3.3. Samples in As-Cast and Heat-Treated Conditions

As the AlZnMg, AlZnMg1Ca, and AlZnMg2Ca were substantially considered in [20] and showed intrinsic as-cast microstructures consistent with (Al)+T and $(Al)+T+(Al, Zn)_4Ca$ phase compositions, these alloys were considered as counterparts in hardness measurements to those containing Fe and Si. The microstructure of the as-cast AlZnMgFeSi alloy (Figure 3a) exhibited clearly defined T phase as bright veins intrinsic to 7xxx alloys, Mg_2Si phase as dark faceted plates, and α-Fe phase as Chinese-script constituents. Indeed, the presence of the latter was not consistent with the calculations, probably due to non-equilibrium solidification conditions, but it is still much more favourable than the Al_3Fe phase. However, the morphology of the α-Fe phase in some places was quite needled and its prevalent size was more than 20 µm, which is believed to be incompatible with further annealing-induced fragmentation. Generally, if both Mg_2Si and α-Fe do not show spheroidization after heat treatment, they will certainly aggravate the ductility, as well as strength, due to lowering the saturation of (Al). On the contrary, the addition of 1% and 2% Ca promotes a sufficient change in the microstructure, which is displayed in Figure 3b,c in the as-cast AlZnMg1CaFeSi and AlZnMg2CaFeSi alloys. It is striking that no Mg_2Si appeared, and thus most Si was likely bonded into the Ca-containing phase. As is shown in [20], the Al_2CaSi_2 may have a coarse faceted morphology specifically in Al-Zn-Mg alloys containing 2% Ca. The presented results also show a significant coarsening of the structure in the AlZnMg2CaFeSi alloy compared to the AlZnMg1CaFeSi alloy. Hence, the latter may have the best response to annealing tuning, since it presents the curved intermetallics with the least linear size. It is prominent that the coarsest area presented magnified in Figure 4a included no Fe, but Ca, Zn, and Si corresponded to the $(Al)+T+(Al, Zn)_4Ca+Al_2CaSi_2$ eutectic mixture. When considering the phase composition of the AlZnMg1CaFeSi alloy that is supported by the elemental maps, Zn is distributed among (Al), T, and $(Al, Zn)_4Ca$ as a dominant element along with Ca. The latter turned out to be successful for binding all the silicon, resulting in the absence of the Mg_2Si phase, while for iron its effect was ambiguous because there was a clearly defined Al_3Fe phase (specified by a triangle in Figures 3b and 4b), and Ca-rich particles probably were $Al_{10}CaFe_2$ phase (specified by a circle in Figures 3b and 4b). Summing up the analysis of the as-cast structures, the most promising alloy, AlZnMg1CaFeSi, was not as perfect as aligned as in the section on the design principles, but outperformed the Ca-free and 2%-Ca bearing counterparts in the size of intermetallics and their morphology.
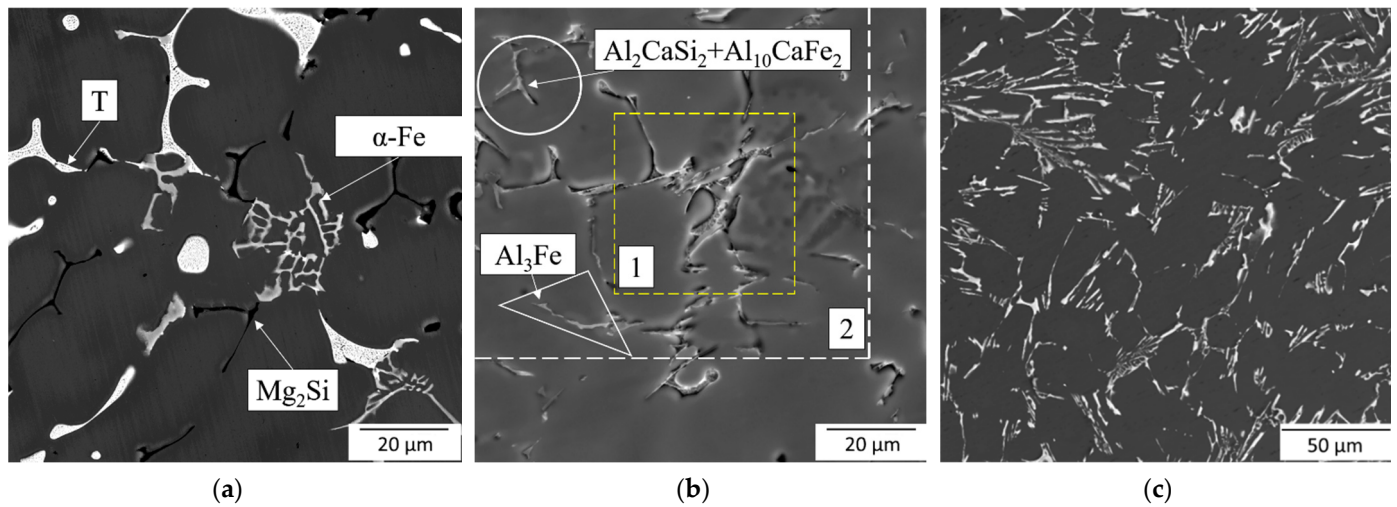
Figure 3. The microstructure of the experimental alloys in an as-cast condition: (**a**) AlZnMgFeSi alloy; (**b**) AlZnMg1CaFeSi alloy (1: area for magnification, see Figure 4a, 2: area for EMPA analysis, see Figure 4b); (**c**) AlZnMg2CaFeSi.
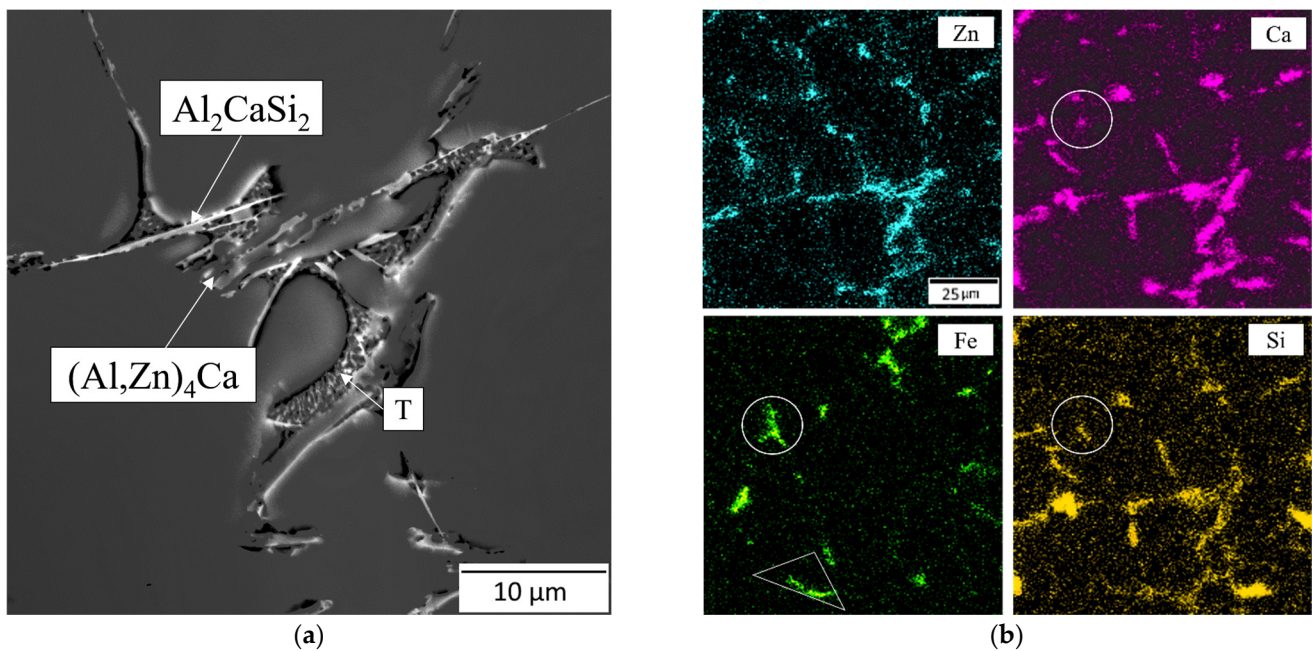

Figure 4. Specific analysis of the as-cast AlZnMg1CaFeSi alloy microstructure: (**a**) magnified section showing the Ca-containing eutectic mixture; (**b**) EMPA elemental mapping on Zn, Ca, Fe, and Si.

The two-step annealing and further quenching of experimental alloys resulted in a complete dissolution of the T phase in (Al). As a result, the base AlZn1Mg alloy becomes a single-phase one, and in other alloys, there was a certain amount of particles containing Ca, Fe, and Si, since these elements are almost insoluble in (Al). The effect of heat treatment on the morphology of these particles was different. When it comes to Fe and Si-free alloys, they exhibited a favourably spheroidized structure, which may be observed in [20]. The structure of the AlZnMgFeSi includes the Mg_2Si phase of a globular morphology, and the Chinese-script α-Fe phase was not sufficiently modified (Figure 5a). The microstructure of the AlZnMg1CaFeSi alloy was more favourable since the particles were distributed more uniformly (Figure 5b). The total number of eutectic particles in this alloy decreased in comparison with the cast state (compare Figures 3b and 5b), primarily due to the dissolution of the T phase. At the same time, the $(Al, Zn)_4Ca$ phase was retained in the structure but acquired a globular morphology. The Fe- and Si-rich phases showed a faceted

shape, but their size was comparable to that of $(Al, Zn)_4Ca$ particles, which was most likely due to fragmentation upon exposure at 520 °C.

The analysis of hardening showed that the $(Al, Zn)_4Ca$ phase brought a decrease in effective Zn content in (Al) and a weakening of ageing response in AlZnMg1Ca, AlZnMg2Ca, and AlZnMg2CaFeSi alloys (170–180 HV in T6) in comparison to the base AlZnMg alloy (~200 HV in T6). A quite similar result was demonstrated for AlZnMgFeSi (185 HV in T6) due to the formation of insoluble Mg_2Si phase, along with lowering of the effective Mg solubility. On the contrary, joint alloying with 1% Ca, Fe, and Si provided appropriate strengthening (195 HV in T6), probably due to a decrease in the amount of $(Al, Zn)_4Ca$ and binding of Ca with Fe and Si-bearing phases.
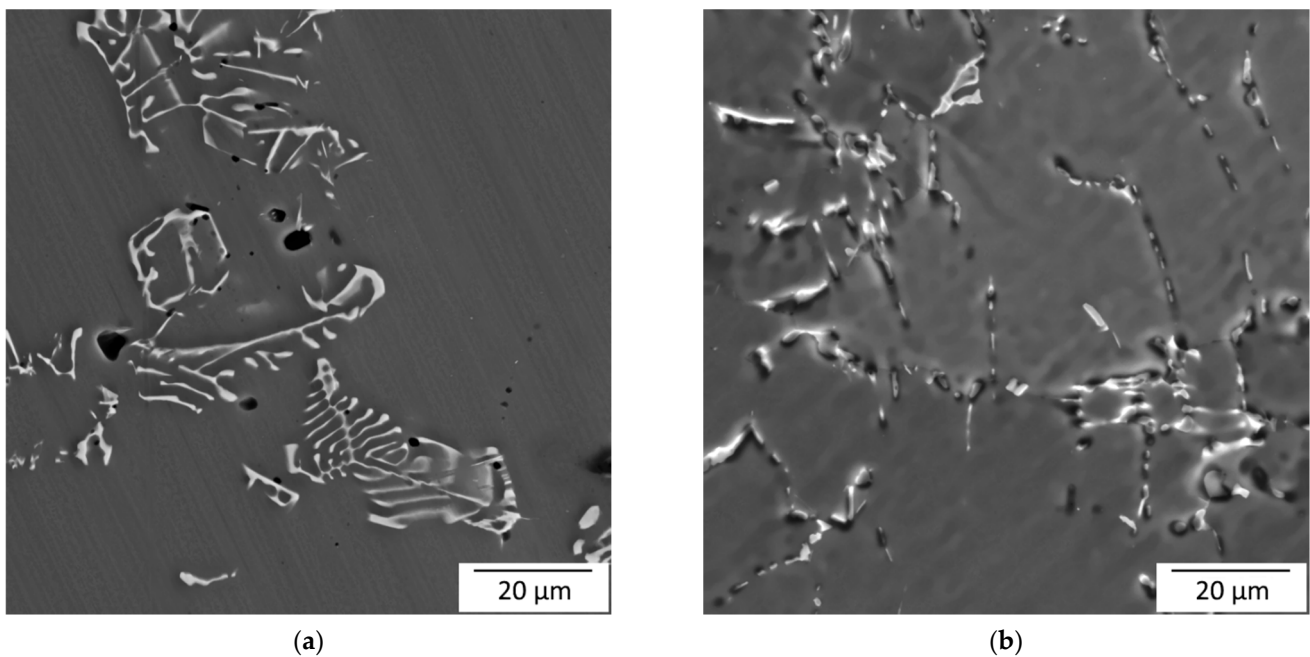

(**a**)   (**b**)

Figure 5. The microstructure of the experimental alloys in the T4 condition: (**a**) AlZnMgFeSi alloy; (**b**) AlZnMg1CaFeSi alloy.

3.4. Deformation and Recycling Feasibility

As is known, the main aggravating effect of Fe and Si in 7xxx alloys is a marked reduction in ductility. For ensuring appropriate plasticity upon rolling, we conducted hot rolling in a solute condition provided by a temperature of 400 °C. It is shown in Figure 6 that the base alloy and both alloys AlZnMgFeSi and AlZnMg1CaFeSi showed quite a similar performance under a hot rolling reduction of ~80%. It may be speculated that as the base alloy was rolled in a high ductility solute condition, the AlZnMgFeSi alloy was successful due to effective breaking of the Chinese-script particles, and the AlZnMg1CaFeSi did not yield as the very fine microstructure provided a uniform load distribution along with the bulk. Contrarily, the AlZnMg2CaFeSi alloy cracked at a reduction of 60%, which was most probably due to its coarse structure.
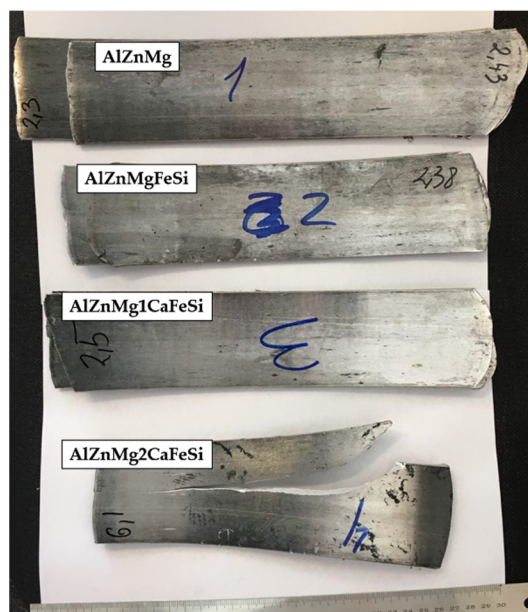
Figure 6. Experimental sheet products.

When it comes to recycling feasibility, it is mostly dependent on the shape of Fe- and Si-bearing intermetallics obtained in the homogenized ingot and final wrought product. The structure of the ingot must favour efficient rolling or extrusion with a high reduction ratio and surface quality in the product. Ultimately, the comparison between AlZnMgFeSi and AlZnMg1CaFeSi reveals the efficiency of joint Ca, Fe, and Si alloying in obtaining a fine microstructure before metal formation comparable to homogenized 6xxx billets manufactured by DC casting. The latter may bring higher cooling rates and uniformity in the structure, due to controlled solidification conditions. As for 6xxx alloys, they are recognized as the main pillars of recyclable aluminium alloys. We analyzed one of the most representative, 6063 alloy (Al-0.45Mg-0.43Si-0.37Fe-0.1Cu-0.07Mn-0.02Ti), as supplied by JSC Aluminum Alloys Plant (Podolsk, Russia), and formulated from secondary stock, like wheels, taint tabor scrap, and drinking cans. Additionally, conductor 1xxx alloys were used for dilution and achieving the nominal grade. First, the alloy's composition is very suitable to be the basis for an AlZnMg1CaFeSi model alloy. Despite the 6063 type grades having a very low strength performance (UTS~200 MPa), they are widespread in fields like construction and automotive, their stream is huge and so appealing to be recycled into high-strength aluminum alloys. When comparing the as-cast structures of the AlZnMg1CaFeSi alloy (Figure3b) and 6063 alloys (Figure 7a), we noticed that the latter contains far fewer intermetallics and that they are mostly needle-shaped related to β-Fe. However, after homogenizing and annealing at 560 °C for 9 h, there is an immense change due to the spheroidization (Figure 7b). The structure qualitatively resembles the pattern presented in Figure 5b of the AlZnMg1CaFeSi alloy in T4 condition and is intrinsic to current recycling-tolerant wrought aluminum alloys. Summing up, it may be preliminary concluded that the new Al-Zn-Mg-Ca-Fe-Si shows promise for being efficiently formulated from Fe- and Si-rich aluminum scrap, including 6xxx series, conductors, and other low-alloyed Al-Fe-Si grades.
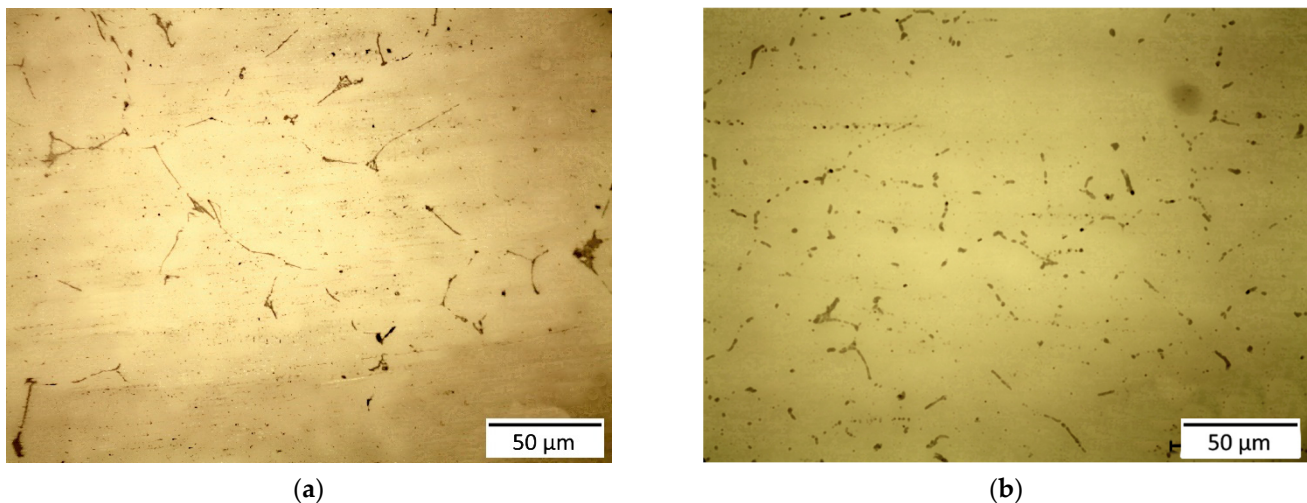
(**a**)

(**b**)

Figure 7. The microstructure of the 6063 alloy as supplied by JSC Aluminum Alloys Plant (Podolsk, Russia): (**a**) as-cast condition; (**b**) annealed condition.

4. Conclusions

In this study, we described an approach to design recycling-tolerant Al-Zn-Mg-Ca aluminum alloys, carried out an experimental study on the Al-Zn-Mg-Ca-Fe-Si alloys, and chose the most promising one, which was then briefly compared with commercial counterparts. The main conclusions are as follows:

1. Recycling-tolerant Al-Zn-Mg-Ca aluminum alloys may be formulated via appropriate alloying and solidification conditions provided they have an as-cast structure including multiphase eutectic with differentiated insoluble intermetallics, which must contain impurities of recycling origin, primarily, Fe and Si. Accordingly, the solidification path and solidus temperature must provide the opportunity for high-temperature heat-treating aimed at tuning the shape of the eutectic phase for favouring performance.

2. The phase composition and solidification path of the Al-Zn-Mg-Ca-Fe-Si alloys showed the presence of multiphase eutectic $(Al)+Al_3Fe+Al_2CaSi_2+Al_4Ca$ under equilibrium solidus of 540 °C. However, a first annealing step at 450 °C was required for the dissolving of the non-equilibrium eutectic solidified at ~480 °C.

3. In comparison to AlZnMgFeSi and AlZnMg2CaFeSi, the AlZnMg1CaFeSi exhibited a sufficiently fine as-cast structure, including differentiated constituents of equilibrium origin Al_3Fe, $Al_{10}CaFe_2$, Al_2CaSi_2, and $(Al.Zn)_4Ca$. After two-step annealing and quenching they were mostly spheroidized, and the non-equilibrium T phase was dissolved in (Al).

4. A synergetic Ca, Fe, and Si effect on the hardening was described. While the Al-Zn-Mg-Ca alloys lose their performance due to Zn dissolution in $(Al, Zn)_4Ca$ phase, joint Ca, Fe, and Si alloying promotes the formation of additional Ca-bearing phases and the increase in effective solute Zn in (Al). The AlZnMg1CaFeSi in the T6 condition possessed a similar hardness value as the base AlZnMg alloy (195 HV vs. 200 HV).

5. The composition of the AlZnMg1CaFeSi alloy may serve as a sufficient basis for the design of new high-strength recycling-tolerant wrought aluminum alloys, since it shows good microstructure, similar to that of 6xxx alloys, excellent hardening response, appropriate processability at metal formation, and may be formulated from Fe- and Si-rich aluminum scrap.

Institutional Review Board Statement: Not applicable.

Informed Consent Statement: Not applicable.

Conflicts of Interest: The authors declare no conflict of interest. The funders had no role in the design of the study; in the collection, analyses, or interpretation of data; in the writing of the manuscript, or in the decision to publish the results.

References

1. Raabe, D.; Tasan, C.C.; Olivetti E.A. Strategies for improving the sustainability of structural metals. *Nature* **2019**, *575*, 64–74, doi:10.1038/s41586-019-1702-5.
2. Trowell, K.A.; Goroshin, S.; Frost, D.L.; Bergthorson, J.M. Aluminum and its role as a recyclable, sustainable carrier of renewable energy. *Appl. Energy* **2020**, *275*, 115112, doi:10.1016/j.apenergy.2020.115112.
3. Haraldsson, J.; Johansson, M.T. Review of measures for improved energy efficiency in production-related processes in the aluminum industry—From electrolysis to recycling. *Renew. Sustain. Energy Rev.* **2018**, *93*, 525–548, doi:10.1016/j.rser.2018.05.043.
4. Wallace, G. Production of secondary aluminum. In *Fundamentals of Aluminium Metallurgy Production, Processing and Applications*, 1st ed.; Lumley, R., Ed.; Woodhead Publishing Ltd.: Cambridge, UK, 2011; pp. 70–82. doi:10.1533/9780857090256.1.70.
5. Das, S.K.; Green, J.A.S.; Kaufman, J.G. The development of recycle-friendly automotive aluminum alloys. *JOM* **2007**, *59*, 47–51, doi:10.1007/s11837-007-0140-2.
6. Cinkilic, E.; Ridgeway, C.D.; Yan, X.; Luo, A.A. A formation map of iron-containing intermetallic phases in recycled cast aluminum alloys. *Metall. Mater. Trans. A* **2019**, *50A*, 5945–5956, doi:10.1007/s11661-019-05469-6.
7. Park, J.O.; Paik, C.H.; Huang, Y.H.; Alkire, R.C. Influence of Fe-Rich intermetallic inclusions on pit initiation on aluminum alloys in aerated NaCl. *J. Electrochem. Soc.* **1999**, *146*, 517–523, doi:10.1149/1.1391637.
8. Belov, N.A.; Aksenov, A.A.; Eskin, D.G. *Iron in Aluminum Alloys: Impurity and Alloying Element*; Taylor & Francis: London, UK, 2002; 360p.
9. Enginsoy, H.M.; Bayraktar, E.; Katundi, D.; Gatamorta, F.; Miskioglu, I. Comprehensive analysis and manufacture of recycled aluminum-based hybrid metal matrix composites through the combined method; sintering and sintering + forging. *Compos. Part B: Eng.* **2020**, *194*, 108040.
10. Hyodo, A.; Bolfarini, C.; Ishikawa, T.T. Chemistry and tensile properties of a recycled AA7050 via spray forming and ECAP/E. *Mater. Res.* **2012**, *15*, 5, 739–748. doi:10.1590/S1516-14392012005000097.
11. She, H.; Chu, W.; Shu, D.; Wang, J.; Sun, B. Effects of silicon content on microstructure and stress corrosion cracking resistance of 7050 aluminum alloy. *Trans. Nonferrous Met. Soc. China* **2014**, *24*, 7, 2307–2313, doi:10.1016/S1003-6326(14)63349-5.
12. Kazeem, A.; Badarulzaman, N.A.; Ali, W.F.F.W. Relating fractographic analysis to yield strength of novel X7475 (Al–Zn–Mg–Cu) alloys produced by recycling aluminum beverage cans. *Mater. Lett.* **2020**, *262*, 127067, doi:10.1016/j.matlet.2019.127067.
13. Kazeem, A.; Badarulzaman, N.A.; Ali, W.F.F.W. Optimization of wear and hardness of Al–Zn–Mg–Cu alloy fabricated from recycled beverage can using response surface methodology. *Sn Appl. Sci.* **2020**, *2*, 1210, doi:10.1007/s42452-020-2836-7.
14. Belov, N.A. Sparingly alloyed high-strength aluminum alloys: Principles of optimization of phase composition. *Met. Sci. Heat Treat.* **2012**, *53*, 420–427, doi:10.1007/s11041-012-9409-3.
15. Akopyan, T.K.; Belov, N.A. Calculation-experimental study of the phase composition of Al-Zn-Mg-(Cu)-Ni-Fe aluminum alloys. *Russ. Metall.* **2013**, *7*, 545–552, doi:10.1134/S0036029513070021.
16. Akopyan, T.K.; Belov, N.A. Approaches to the design of the new high-strength casting aluminum alloys of 7xxx series with high iron content. *Non-Ferr. Met.* **2016**, *1*, 20–27, doi:10.17580/nfm.2016.01.04.
17. Belov, N.A.; Naumova, E.A.; Akopyan, T.K.; Doroshenko, V.V. Phase diagram of the Al-Ca-Fe-Si system and its application for the design of aluminum matrix composites. *JOM* **2018**, *70*, 2710–2715, doi:10.1007/s11837-018-2948-3.
18. Belov, N.; Akopyan, T.; Korotkova, N.; Murashkin, M.; Timofeev, V.; Fortuna, A. Structure and Properties of Ca and Zr Containing Heat ResistantWire Aluminum Alloy Manufactured by Electromagnetic Casting. *Metals* **2021**, *11*, 236, doi:10.3390/met11020236.
19. Shurkin, P.K.; Dolbachev, A.P.; Naumova, E.A.; Doroshenko, V.V. Effect of iron on the structure, hardening and physical properties of the alloys of the Al-Zn-Mg-Ca system. *Tsvetnye Met.* **2018**, *5*, 69–77, doi:10.17580/tsm.2018.05.10.
20. Shurkin, P.K.; Belov, N.A.; Musin, A.F.; Samoshina, M.E. Effect of calcium and silicon on the character of solidification and strengthening of the Al–8% Zn–3% Mg Alloy. *Phys. Met. Met.* **2020**, *121*, 135–142, doi:10.1134/S0031918X20020155.
21. Thermo-Calc Software—Computational Materials Engineering. Available online: http://www.thermocalc.com (accessed on 1 February 2021).
22. Shu, W.X.; Hou, L.G.; Zhang, C.; Zhang, F.; Liu, J.C.; Liu, J.T.; Zhuang, L.Z.; Zhang, J.S. Tailored Mg and Cu contents affecting the microstructures and mechanical properties of high-strength Al-Zn-Mg-Cu alloys. *Mater. Sci. Eng. A* **2016**, *657*, 269–283, doi:10.1016/j.msea.2016.01.039.
23. Chen, Z.; Mo, Y.; Nie, Z. Effect of Zn content on the microstructure and properties of super-high-strength Al-Zn-Mg-Cu alloys. *Metall. Mater. Trans.* **2013**, *44A*, 3910–3920, doi:10.1007/s11661-013-1731-x.
24. Shin, J.; Kim, T.; Kim, D.E.; Kim, D.; Kim, K. Castability and mechanical properties of new 7xxx aluminum alloys for automotive chassis/body applications. *JALCOM* **2017**, *698*, 577–590, doi:10.1016/j.jallcom.2016.12.269.

25. The Aluminium Association, International Alloy Designations and Chemical Composition Limits for Wrought Aluminium and Wrought Aluminium Alloys. The Aluminium Association. Available online: https://www.aluminum.org/sites/default/files/Teal%20Sheets.pdf (accessed on 1 February 2021).

26. Shurkin, P.K.; Belov, N.A.; Musin, A.F.; Aksenov, A.A. Novel high-strength casting Al−Zn−Mg−Ca−Fe aluminum alloy without heat treatment. *Russ. J. Non-Ferr. Met.* **2020**, *61*, 179–187, doi:10.3103/S1067821220020121.